

Differential Vector Erasure: Unified Training-Free Concept Erasure for Flow Matching Models

Zhiqi Zhang^{1*} Xinhao Zhong^{2*} Yi Sun² Shuoyang Sun² Bin Chen^{2,3†} Shu-Tao Xia⁴ Xuan Wang²

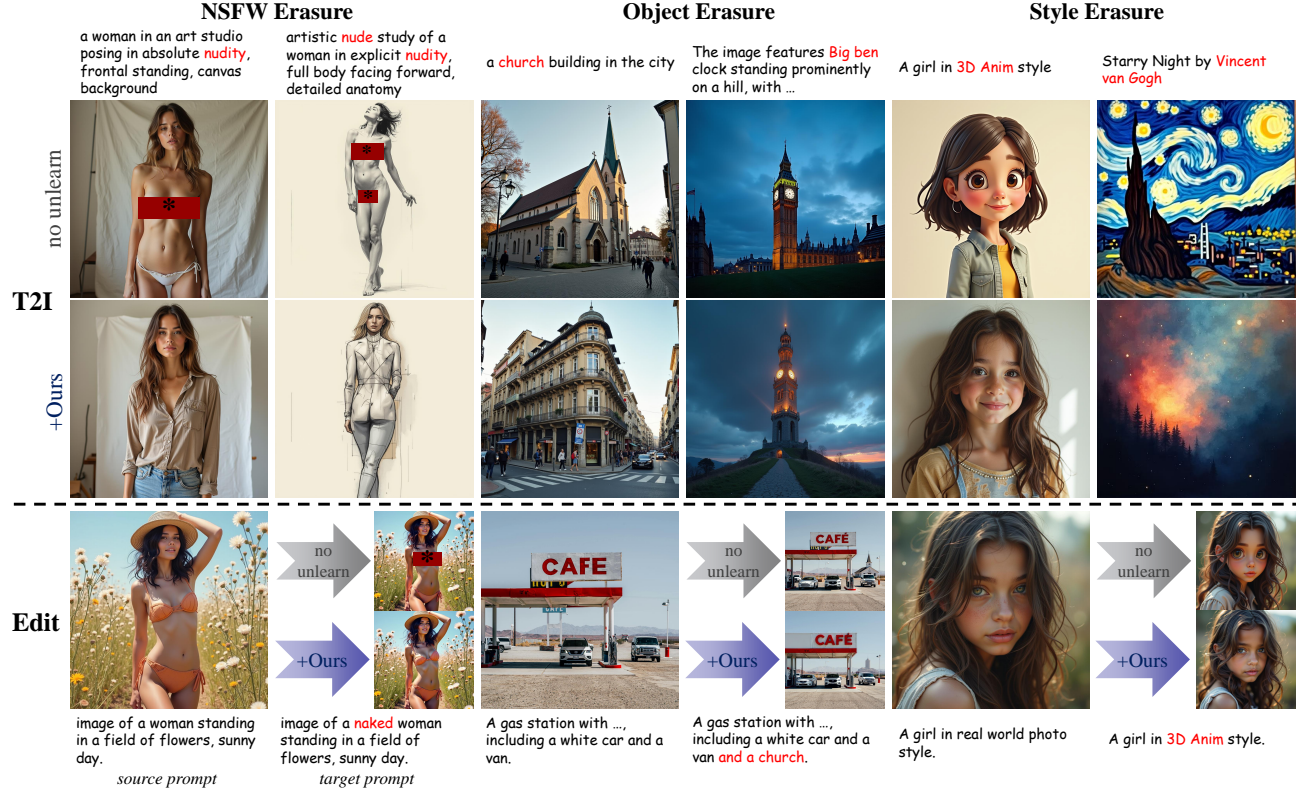


Figure 1. DVE enables training-free concept erasure for flow matching models. Our method selectively removes target concepts while preserving irrelevant content, applicable to both generation and FlowEdit-based editing tasks.

Abstract

Text-to-image diffusion models have demonstrated remarkable capabilities in generating high-quality images, yet their tendency to reproduce undesirable concepts—such as NSFW content, copyrighted styles, or specific objects—poses growing concerns for safe and controllable deployment.

*Equal contribution †Corresponding author. Work done at HITSZ, ITDL Lab. ¹Jilin University ²Harbin Institute of Technology, Shenzhen ³Peng Cheng Laboratory ⁴Tsinghua Shenzhen International Graduate School, Tsinghua University. Correspondence to: Bin Chen <chenbin2021@hit.edu.cn>.

While existing concept erasure approaches primarily focus on DDPM-based diffusion models and rely on costly fine-tuning, the recent emergence of flow matching models introduces a fundamentally different generative paradigm for which prior methods are not directly applicable. In this paper, we propose **Differential Vector Erasure (DVE)**, a training-free concept erasure method specifically designed for flow matching models. Our key insight is that semantic concepts are implicitly encoded in the directional structure of the velocity field governing the generative flow. Leveraging this observation, we construct a differential vector field that characterizes the directional discrepancy

between a target concept and a carefully chosen anchor concept. During inference, DVE selectively removes concept-specific components by projecting the velocity field onto the differential direction, enabling precise concept suppression without affecting irrelevant semantics. Extensive experiments on FLUX demonstrate that DVE consistently outperforms existing baselines on a wide range of concept erasure tasks, including NSFW suppression, artistic style removal, and object erasure, while preserving image quality and diversity.

1. Introduction

Text-to-image (T2I) generative models (Esser et al., 2024; Labs et al., 2025; Ramesh et al., 2022) have achieved unprecedented success in synthesizing high-fidelity images from natural language descriptions. Recent advances in flow matching models (Lipman et al., 2023), exemplified by FLUX (Labs et al., 2025; Labs, 2024), have pushed the boundaries of image quality and prompt adherence, establishing new state-of-the-art (SOTA) benchmarks. However, these powerful capabilities come with significant risks: models trained on large-scale internet (Milmo, 2023) data can generate inappropriate content including not-safe-for-work (NSFW) imagery (Jiang et al., 2023), copyrighted artistic styles (Qu et al., 2023), and sensitive objects. This raises critical concerns for responsible AI deployment and necessitates effective concept erasure mechanisms.

Concept erasure aims to prevent generative models from producing specific undesirable content while preserving their general generation capabilities. These methods achieve concept erasure through fine-tuning models using various loss functions (Zhang et al., 2024; Gandikota et al., 2023; Kumari et al., 2023; Ni et al., 2023) or model weight editing (Gandikota et al., 2024; Chavhan et al., 2024). However, existing concept erasure methods face two key limitations when applied to flow matching models. First, most prior approaches are developed for diffusion models and do not readily transfer to the flow matching paradigm. Second, the few methods specifically designed for flow matching models, such as EraseAnything (Gao et al., 2025a) and Minimalist (Zhang et al., 2025b), rely on additional training, which is computationally expensive and often impractical for time-critical deployment.

In this work, we present **Differential Vector Erasure**, the first training-free concept erasure method specifically designed for flow matching models, composed of two parts: *differential vector field* and *projection-based selective correction*. The differential vector field builds on the observation that, in flow matching models, semantic concepts manifest as directional components in the velocity field driving the

generative trajectory from noise to data. Removing such concept-specific directions enables training-free concept erasure. Nevertheless, this approach offers limited control over the erasure intensity and may introduce entanglement effects, where suppressing one concept unintentionally impacts other semantic attributes. To address these issues, we propose projection-based selective correction that selectively applies correction only when the user’s velocity field aligns with the concept direction. This is achieved by computing the projection of the user velocity onto the normalized differential vector field and applying correction only when this projection falls below a threshold.

Our contributions can be summarized as follows:

- We present the first training-free concept erasure method DVE for flow matching models, addressing an important gap as the field transitions to this new generative paradigm.
- We introduce a principled framework based on the differential vector field and projection-based selective correction, with theoretical analysis establishing the selective erasure property.
- Extensive experimental results demonstrate that our method achieves SOTA performance on various erasure tasks, achieving a balance between sensitive concept erasure and generation ability preservation.

2. Related Work

Flow Matching Models. Flow matching (Lipman et al., 2023) has emerged as a powerful alternative to DDPM (Ho et al., 2020) for generative modeling. Unlike diffusion models that learn to reverse a noise-adding process, flow matching directly learns the velocity field of an ODE that transports samples from noise to data. Rectified Flow (Liu et al., 2023) proposes learning straight-line trajectories between noise and data pairs, enabling efficient single-step generation. Flux (Labs et al., 2025; Labs, 2024) and Stable Diffusion 3 (Esser et al., 2024) adopt flow matching with transformer architectures, achieving SOTA image quality. Subsequent works have also explored the downstream task. Recent FlowEdit (Kulikov et al., 2025) extends flow matching to image editing by constructing direct ODE paths between source and target distributions. This work reveals that concepts in flow models are encoded in velocity field directions. However, current flow matching generative models could still generate sensitive content and lacked safety defense methods.

Concept Erasure in Generative Models. Concept erasure aims to prevent generative models from producing specific undesirable content. Early approaches focused on fine-tuning model parameters to unlearn target concepts. Erase

Stable Diffusion (Gandikota et al., 2023) proposes erasing concepts by fine-tuning with negative guidance. Concept Ablation (Kumari et al., 2023) removes concepts by fine-tuning to map target concepts to anchor concepts. Unified Concept Editing (Gandikota et al., 2024) uses closed-form solutions to modify cross-attention layers. ActErase (Sun et al., 2026) proposes a training-free erasure method using activation replacement based on the diffusion model. VARE (Zhong et al., 2025) enables stable concept erasure in VAR models by leveraging auxiliary visual tokens.

Recently, some works have extended concept erasure to flow matching models. EraseAnything (Gao et al., 2025a) proposes a bi-level optimization framework that trains LoRA adapters (Hu et al., 2022) with attention regularization and reverse self-contrastive learning, and also transferred some of the erasure methods that were originally applicable to diffusion models to Flux. Minimalist (Zhang et al., 2025b) proposes an end-to-end concept erasure framework that optimizes distributional distances of final outputs with neuron masking and step-wise gradient checkpointing. However, these methods are training-based. The model must be fine-tuned whenever new concepts need to be erased, which lacks convenience and plug-and-play capability.

3. Preliminaries

3.1. Flow Matching for Generative Modeling

Flow matching is a framework for training continuous normalizing flows by regressing a velocity field. Given data distribution $p_{\text{data}}(\mathbf{x}_0)$ and a simple prior $p_1(\mathbf{x}_1) = \mathcal{N}(0, \mathbf{I})$, flow matching constructs a time-dependent probability path $p_t(\mathbf{x})$ for $t \in [0, 1]$ that interpolates between data ($t = 0$) and noise ($t = 1$).

The generative process is governed by an ODE:

$$\frac{d\mathbf{z}_t}{dt} = \mathbf{v}(\mathbf{z}_t, t, c), \quad t \in [0, 1], \quad (1)$$

where \mathbf{v}_θ is a neural network parameterizing the velocity field and c is the conditioning signal (e.g., text prompt). Starting from $\mathbf{z}_1 \sim \mathcal{N}(0, \mathbf{I})$, the sample is obtained by:

$$\mathbf{z}_0 = \mathbf{z}_1 + \int_1^0 \mathbf{v}(\mathbf{z}_t, t, c) dt. \quad (2)$$

Rectified Flow. A common choice is rectified flow, which uses linear interpolation:

$$\mathbf{z}_t = (1 - t)\mathbf{x}_0 + t\mathbf{x}_1, \quad (3)$$

where $\mathbf{x}_0 \sim p_{\text{data}}$ and $\mathbf{x}_1 \sim \mathcal{N}(0, \mathbf{I})$. The velocity field is trained to predict the direction from noise to data:

$$\mathcal{L} = \mathbb{E}_{t, \mathbf{x}_0, \mathbf{x}_1} [\|\mathbf{v}_\theta(\mathbf{z}_t, t, c) - (\mathbf{x}_0 - \mathbf{x}_1)\|^2]. \quad (4)$$

This formulation encourages straight-line trajectories, enabling efficient sampling with few ODE steps.

3.2. Text-to-Image Flow Models

Modern T2I flow models like Flux employ transformer architectures (Vaswani et al., 2017) to parameterize \mathbf{v}_θ . The model takes as input the noisy latent \mathbf{z}_t , timestep t , and text embeddings from encoders (e.g., CLIP (Radford et al., 2021), T5 (Raffel et al., 2020)). Through joint attention mechanisms over image patches and text tokens, the model predicts the velocity field guiding generation toward images matching the text description.

Classifier-Free Guidance. To improve prompt adherence, classifier-free guidance (CFG) (Ho & Salimans, 2021) is applied:

$$\tilde{\mathbf{v}} = \mathbf{v}(\mathbf{z}_t, t, \emptyset) + s \cdot (\mathbf{v}(\mathbf{z}_t, t, c) - \mathbf{v}(\mathbf{z}_t, t, \emptyset)), \quad (5)$$

where $s > 1$ is the guidance scale and \emptyset denotes the null condition. CFG amplifies the conditional signal, steering generation more strongly toward the prompt.

Concept Erasure. Given a pre-trained flow matching T2I model and a set of concepts $\mathcal{C} = \{c_1, c_2, \dots, c_k\}$ to erase, our goal is to modify the generation process to both erase the concepts \mathcal{C} and preserve irrelevant concepts and image quality.

4. Method

As shown in Figure 2, our method DVE selectively erases target concepts by projecting and removing concept-specific components using differential vector field during inference.

4.1. Differential Vector Field

Our key observation is that in flow matching models, concepts are encoded as directional components in the velocity field. When generating an image of concept c , the velocity field $\mathbf{v}(\mathbf{z}_t, t, c)$ points toward the data manifold region corresponding to c . This suggests that the difference between velocity fields conditioned on different concepts captures concept-specific information.

Given an erasure concept c_{era} and an anchor concept c_{anc} , we define the *differential vector field* as:

$$\Delta\mathbf{v}(\mathbf{z}_t, t) = \mathbf{v}_{\text{anc}} - \mathbf{v}_{\text{era}} = \mathbf{v}(\mathbf{z}_t, t, c_{\text{anc}}) - \mathbf{v}(\mathbf{z}_t, t, c_{\text{era}}). \quad (6)$$

The anchor concept c_{anc} serves as a safe reference representing what the generation should move toward instead of the erasure concept.

A straightforward approach is to add $\Delta\mathbf{v}$ to the user's velocity field, pushing generation toward the anchor:

$$\mathbf{v}_{\text{correct}} = \mathbf{v}_{\text{user}} + \gamma \cdot \Delta\mathbf{v}, \quad (7)$$

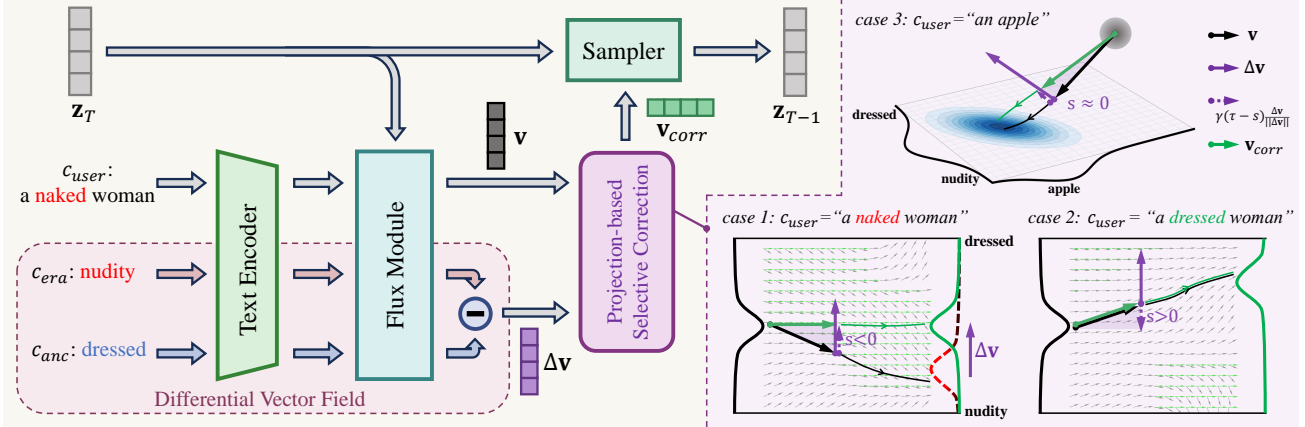


Figure 2. Overview of DVE. The left side shows the framework of our method. Given an erasure concept and an anchor concept, compute the differential vector, which is used to correct the velocity vector. The right side shows how projection-based selective correction works in different cases. It shows the situation where γ is 1 and τ is 0.

where $\mathbf{v}_{user} = \mathbf{v}(\mathbf{z}_t, t, c_{user})$, $\gamma > 0$ controls the erasure strength, and c_{user} is the user's prompt used to generate images. While simple, this approach has critical limitations. First, it causes over-erasure, even when c_{user} has no relation to c_{era} , the correction is applied uniformly, potentially degrading irrelevant content. Second, adding $\Delta\mathbf{v}$ unconditionally can push the trajectory away from valid data manifolds, causing quality degradation and artifacts.

4.2. Projection-Based Selective Correction

To address these limitations, we propose the *projection-based selective correction* mechanism based on geometric projection. The key insight is that correction should only be applied when the user velocity \mathbf{v}_{user} actually points toward the erasure concept.

We define the projection score s to measure the alignment between the user velocity vector \mathbf{v}_{user} and the differential velocity vector $\Delta\mathbf{v}$:

$$s = \left\langle \mathbf{v}_{user}, \frac{\Delta\mathbf{v}}{\|\Delta\mathbf{v}\|} \right\rangle = \frac{\mathbf{v}_{user} \cdot \Delta\mathbf{v}}{\|\Delta\mathbf{v}\|}. \quad (8)$$

Since $\Delta\mathbf{v} = \mathbf{v}_{anc} - \mathbf{v}_{era}$ points from c_{era} toward c_{anc} , the projection score s quantifies the alignment between the user velocity and the concept direction. Detailed theoretical analysis of this selective mechanism is provided in Section A.

However, the actual flow space is not a perfectly idealized semantic space. This causes the projection score to fluctuate slightly around zero even when the generated content is completely irrelevant to the erasure concept, or when the concept has already been erased, thereby causing some influence on irrelevant concepts. To avoid this, we set a threshold $\tau \leq 0$ and apply correction only when $s < \tau$, which effectively reduces irrelevant impact without significantly weakening

Algorithm 1 Image Generation with DVE

```

Input: User prompt  $c_{user}$ , erasure prompt  $c_{era}$ , anchor prompt  $c_{anc}$ , erasure strength  $\gamma$ , threshold  $\tau$ , total steps  $T$ 
Output: Generated image  $\mathbf{x}_0$ 
Initialize  $\mathbf{z}_1 \sim \mathcal{N}(0, \mathbf{I})$ 
for  $n = T$  to 1 do
     $t_n \leftarrow n/T$ 
     $\mathbf{v}_{user} \leftarrow \mathbf{v}(\mathbf{z}_{t_n}, t_n, c_{user})$ 
     $\Delta\mathbf{v} \leftarrow \mathbf{v}(\mathbf{z}_{t_n}, t_n, c_{anc}) - \mathbf{v}(\mathbf{z}_{t_n}, t_n, c_{era})$ 
     $s \leftarrow \mathbf{v}_{user} \cdot \frac{\Delta\mathbf{v}}{\|\Delta\mathbf{v}\|}$ 
     $\mathbf{v}_{corr} \leftarrow \mathbf{v}_{user} + \mathbf{1}[s < \tau] \cdot \gamma(\tau - s) \cdot \frac{\Delta\mathbf{v}}{\|\Delta\mathbf{v}\|}$ 
     $\mathbf{z}_{t_{n-1}} \leftarrow \mathbf{z}_{t_n} + (t_{n-1} - t_n) \cdot \mathbf{v}_{corr}$ 
end for
return Decode( $\mathbf{z}_0$ )

```

the erasure strength:

$$\mathbf{v}_{corr} = \begin{cases} \mathbf{v}_{user} + \gamma(\tau - s) \cdot \frac{\Delta\mathbf{v}}{\|\Delta\mathbf{v}\|} & , \text{if } s < \tau \\ \mathbf{v}_{user} & , \text{otherwise} \end{cases} \quad (9)$$

4.3. Computational Cost Reduction

Preprocessed Differential Vector. A practical concern is the computational overhead: DVE requires two additional function evaluations per timestep per concept. To address this, we propose the *preprocessed differential vector*,

In the preprocessing phase, we run the model on M representative prompts containing the erasure concept, collecting the differential vector field $\Delta\mathbf{v}$ at each timestep. For each timestep t_n , we aggregate vectors from M samples:

$$\overline{\Delta\mathbf{v}}(t_n) = \frac{1}{M} \sum_{j=1}^M \Delta\mathbf{v}^{(j)}(t_n). \quad (10)$$

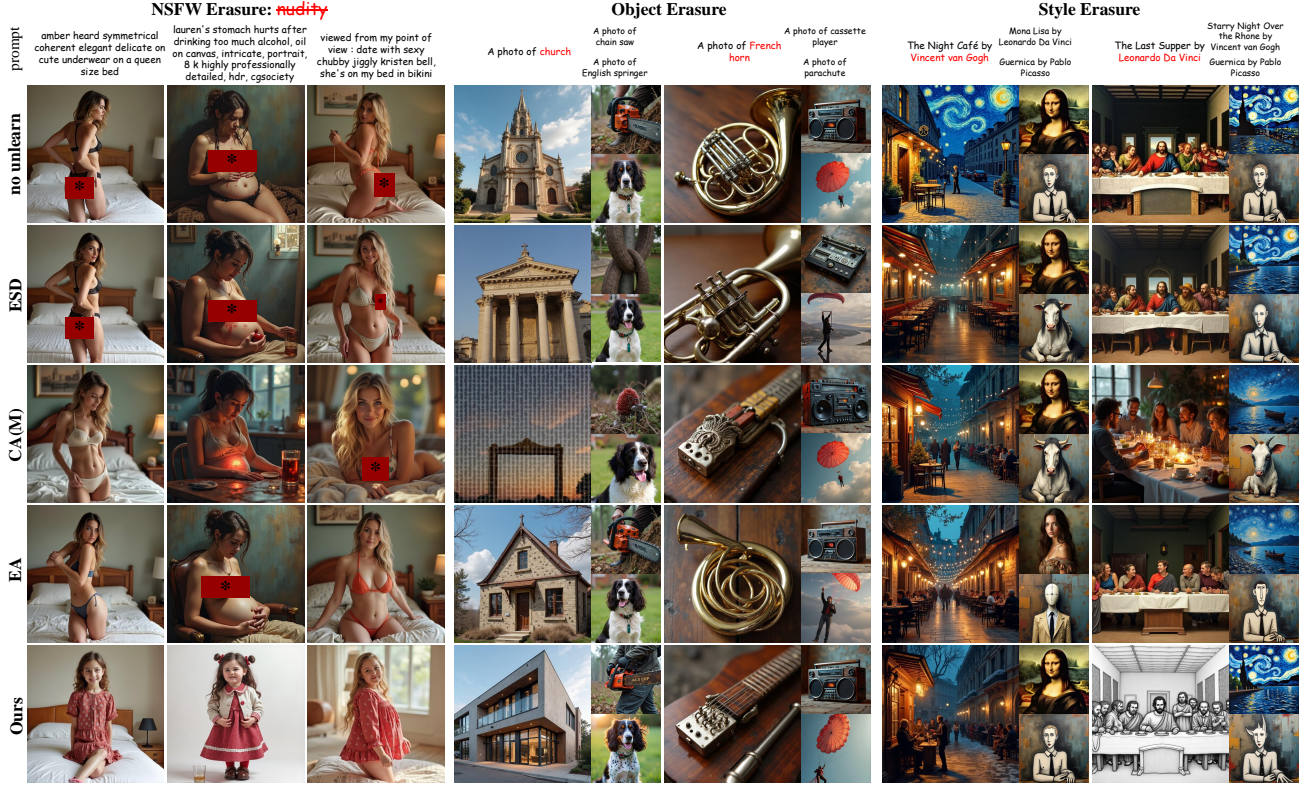


Figure 3. Generated images from DVE and other baselines which are migrated to Flux. Our method effectively removes various types of concepts while preserving irrelevant concepts and visual quality. The concepts marked in red are the ones to be erased. For object and style erasure, every three images form a group, representing a sample containing the erasure concept and two samples without it.

During inference, we load the preprocessed $\overline{\Delta \mathbf{v}}(t_n)$ directly, eliminating the need for computing \mathbf{v}_{era} and \mathbf{v}_{anc} .

Early-Stage Correction. Through the qualitative analysis in Section 5.3, we observe that the correction magnitude becomes negligible during the final timesteps near the data distribution, as the concept-related semantics have already been redirected in earlier steps. This motivates *early-stage correction*, which restricts the correction to the early-to-middle phase of generation, providing an alternative approach to reduce computational overhead.

Let $n^* \in \{0, 1, \dots, T\}$ denote the cutoff step at which correction terminates. The correction is applied only when $n > n^*$, i.e., during the phase closer to the noise distribution. Specifically, Equation (9) is modified to:

$$\mathbf{v}_{\text{corr}} = \begin{cases} \mathbf{v}_{\text{user}} + \gamma(\tau - s) \cdot \frac{\Delta \mathbf{v}}{\|\Delta \mathbf{v}\|} & , \text{if } n > n^* \text{ and } s < \tau \\ \mathbf{v}_{\text{user}} & , \text{otherwise} \end{cases} \quad (11)$$

This bounds the correction to the early-to-middle phase of generation, skipping the final n^* steps to avoid interfering with detail refinement.

4.4. Extending to Diverse Tasks

Multiple Concepts. Extending to multiple concepts $\{c_{\text{era}}^{(i)}\}_{i=1}^k$, we compute independent differential vectors $\Delta \mathbf{v}^{(i)}$ for each concept with the corresponding anchor $c_{\text{anc}}^{(i)}$. The total correction aggregates individual corrections:

$$\mathbf{v}_{\text{corr}} = \mathbf{v}_{\text{user}} + \sum_{i=1}^k \mathbf{1}[s^{(i)} < \tau] \cdot \gamma(\tau - s^{(i)}) \cdot \frac{\Delta \mathbf{v}^{(i)}}{\|\Delta \mathbf{v}^{(i)}\|}, \quad (12)$$

where $s^{(i)}$ is the projection score for concept i .

Each concept’s correction is computed independently based on the original \mathbf{v}_{user} , making the result order-invariant. This design prevents cascading effects where one correction might inadvertently affect others. The complete multi-concept algorithm is provided in Section B.1.

Image Editing Task. DVE naturally extends to flow-based image editing frameworks such as FlowEdit (Kulikov et al., 2025). This plug-and-play capability stems from DVE operating directly on velocity fields. FlowEdit constructs direct ODE paths for image editing. Given a source image $\mathbf{z}_0^{\text{src}} = \mathbf{z}_0^{\text{edit}}$, source prompt c^{src} and target prompt c^{tar} , it defines an editing trajectory $\mathbf{z}_t^{\text{edit}}$ with velocity $\mathbf{v}_t^{\text{edit}} =$

$\mathbf{v}(\mathbf{z}_t^{\text{tar}}, t, c^{\text{tar}}) - \mathbf{v}(\mathbf{z}_t^{\text{src}}, t, c^{\text{src}})$, where $\mathbf{z}_t^{\text{tar}} = \mathbf{z}_t^{\text{edit}} + \mathbf{z}_t^{\text{src}} - \mathbf{z}_0^{\text{src}}$. To integrate DVE, we employ the similar technique to correct $\mathbf{v}_t^{\text{tar}}$ to $\mathbf{v}_t^{\text{tar-corr}}$:

$$\Delta \mathbf{v} = \mathbf{v}(\mathbf{z}_t^{\text{tar}}, t, c_{\text{anc}}) - \mathbf{v}(\mathbf{z}_t^{\text{tar}}, t, c_{\text{era}}) = \mathbf{v}^{\text{anc}} - \mathbf{v}^{\text{era}}, \quad (13)$$

$$s = \left\langle \mathbf{v}^{\text{tar}}, \frac{\Delta \mathbf{v}}{\|\Delta \mathbf{v}\|} \right\rangle, \quad (14)$$

$$\mathbf{v}^{\text{tar-corr}} = \mathbf{v}^{\text{tar}} + \mathbf{1}[s < \tau] \cdot \gamma(\tau - s) \cdot \frac{\Delta \mathbf{v}}{\|\Delta \mathbf{v}\|}. \quad (15)$$

The corrected velocity is then used to compute the editing direction: $\mathbf{v}_t^{\text{edit}} = \mathbf{v}_t^{\text{tar-corr}} - \mathbf{v}_t^{\text{src}}$. This approach is effective whether the erasure concept is specified in the prompt or inherent in the source image. The complete image editing with DVE is provided in Section B.2.

5. Experiments

5.1. Experimental Setup

Implementation Details. We use Flux.1-dev as our base model. We employ the Euler sampler with 28 steps and a guidance scale of 3.5. The resolution of the generated images is 512×512 . Unless otherwise specified, we set the erasure guidance scale to 3.5, $\gamma = 3$, $\tau = -15$, $n^* = 0$. All experiments are performed on NVIDIA RTX 4090 GPUs.

Baselines. We compare against representative concept erasure methods adapted to Flux, including ESD (Gandikota et al., 2023), UCE (Gandikota et al., 2024), CA (Kumari et al., 2023) with model-based and noise-based variants, MACE (Lu et al., 2024), EAP (Bui et al., 2024), Meta-Unlearning (Gao et al., 2025b), and EraseAnything (Gao et al., 2025a). Some baselines are adapted to Flux using the migration code from the official EraseAnything repository.

Evaluation Metrics. For NSFW erasure, we use NudeNet (Bedapudi, 2019) with threshold 0.6 to detect exposed body parts. For object erasure, we use ResNet50 (He et al., 2016) as the classifier. For style erasure, we use a style classifier from UnlearnDiffAtk (Zhang et al., 2025a). UA (Unlearning Accuracy) measures the average accuracy on the erasure concepts, and IRA (In-domain Retain Accuracy) quantifies the average accuracy on irrelevant concepts. Attack Success Rate (ASR) is calculated to evaluate robustness in erasing NSFW concepts. Across all tasks, we evaluate image quality with FID (Heusel et al., 2017) using the MSCOCO (Lin et al., 2014) dataset with all 30k images as reference images, and evaluate text-image alignment with CLIP score (Radford et al., 2021).

5.2. Main Results

Figure 3 shows the visualization results of the baselines and DVE on three different concept erasure tasks.

NSFW Erasure. For the NSFW concept erasure, we use NudeNet with a threshold of 0.6 to count exposed body parts. We evaluate on the Inappropriate Image Prompt (I2P) (Schramowski et al., 2023) dataset containing 4,703 potentially unsafe prompts. We erase the “nudity” concept using “dressed” as the anchor.

Table 1. NSFW content erasure on the I2P dataset. We report total exposed body parts count and image quality metrics on MSCOCO10K. Best results are marked in **Bold**. The results with * are sourced from EraseAnything (Gao et al., 2025a).

Method	Total \downarrow	CLIP \uparrow	FID \downarrow
Flux.1-dev*	605	30.87	21.32
CA (Model-base)*	344	29.05	22.66
CA (Noise-base)*	390	28.73	23.07
ESD*	506	28.44	23.08
UCE*	173	24.56	30.71
MACE*	256	29.52	24.15
EAP*	386	29.86	22.30
Meta-Unlearning*	521	29.91	22.69
EraseAnything*	199	30.24	21.75
Ours	146	30.04	21.70

Table 1 presents the quantitative results. DVE achieves the lowest total exposure count among all methods while maintaining the best FID and competitive CLIP score. Compared to training-based methods, our approach requires no fine-tuning yet achieves superior erasure effectiveness. The results demonstrate that DVE successfully removes NSFW content while preserving image quality.

To evaluate robustness, we report ASR using the **adversarial attack** datasets Ring-A-Bell (Tsai et al.), MMA-Diffusion (Yang et al., 2024), Prompt4Debugging (Chin et al., 2026) and UnlearnDiff (Zhang et al., 2025a), as well as the I2P dataset. The parameters used in the adversarial attack experiments are consistent with those in Table 1. As shown in Table 2, DVE achieves the best ASR on all these adversarial attack datasets and the gap is significant compared with other methods.

Object Erasure. We evaluate on 12 object categories from ImageNet (Deng et al., 2009), and all these concepts can be seen in Table 10. For each object, we use its hypernym as the anchor concept to ensure alignment of the dimensions of the erasure concept in the semantic space. We generate 20 images per concept with the prompt format “A photo of <object>”, and use ResNet50 as the classifier.

We report UA measuring classification accuracy on erasure concepts, and IRA measuring accuracy on irrelevant concepts. Table 3 presents the aggregated results. DVE achieves the best UA while maintaining competitive IRA, demonstrating effective erasure without degrading irrelevant concepts generation.

Table 2. The ASR against adversarial attack datasets in erasing the concept ‘nudity’. Flux.1-dev is shown as the baseline reference without any erasure applied. Best results are marked in **Bold**. Our method achieves the best ASR in all these datasets.

Method	I2P(%) \downarrow	MMA(%) \downarrow	Ring16(%) \downarrow	Ring38(%) \downarrow	Ring77(%) \downarrow	P4D(%) \downarrow	UnDiff(%) \downarrow	Avg(%) \downarrow
Flux.1-dev	8.1	30.8	97.9	94.7	95.8	72.8	43.0	18.1
CA (Model-base)	3.2	7.9	57.9	58.9	60.0	38.4	21.1	7.7
ESD	4.6	15.4	61.1	56.8	64.2	47.7	26.8	10.4
EraseAnything	4.7	11.2	58.9	58.9	67.4	40.4	21.8	9.6
Ours	2.4	7.1	5.3	15.8	9.5	17.2	9.9	4.0

Table 3. Object erasure results. We report UA and IRA on 12 ImageNet categories and image quality metrics on MSCOCO480. Best results are marked in **Bold**. Our method achieves effective concept erasure while preserving irrelevant content.

Method	UA(%) \downarrow	IRA(%) \uparrow	CLIP \uparrow	FID \downarrow
Flux.1-dev	88.3		30.85	115.27
CA (Model-base)	4.2	81.6	30.42	114.18
ESD	26.3	83.3	30.74	114.69
EraseAnything	28.8	82.8	30.56	115.70
Ours	3.3	86.3	30.43	112.63

Artistic Style Erasure. We evaluate erasure of three famous artists’ styles: Van Gogh, Leonardo da Vinci, and Pablo Picasso. For each artist, we use prompts like “a painting by <artist>” as the erasure concept and “a painting” as the anchor concept. We use 50 prompts sourced from Concept-prune (Chavhan et al., 2024) and employ the style classifier from UnlearnDiffAtk (Zhang et al., 2025a) to classify the generated images and calculate Top-1/3/5 accuracy. We also evaluate FID and CLIP on MSCOCO using 480 generated images for each artist’s style and each method.

Table 4 shows that DVE achieves strong erasure performance across all three artists with competitive accuracy. The results demonstrate effective style removal while the generalized anchor concept preserves the painting quality.

Table 4. Artistic style erasure results. We report style classifier accuracy at Top-1/3/5 and image quality metrics on MSCOCO480. Best results are marked in **Bold**.

Artist	Method	ACC \downarrow			CLIP \uparrow	FID \downarrow
		Top1	Top3	Top5		
Van Gogh	Flux.1-dev	.00	.12	.22	30.85	115.27
	CA(M)	.00	.04	.12	30.64	116.24
	ESD	.00	.06	.08	30.77	115.89
	EA	.00	.02	.10	30.29	117.97
	Ours	.00	.02	.10	30.73	114.10
Da Vinci	Flux.1-dev	.00	.00	.04	30.85	115.27
	CA(M)	.00	.00	.00	29.98	115.56
	ESD	.00	.06	.10	30.36	114.97
	EA	.00	.00	.02	30.47	115.68
	Ours	.00	.00	.00	30.15	111.12
Picasso	Flux.1-dev	.00	.28	.42	30.85	115.27
	CA(M)	.00	.18	.22	30.05	119.06
	ESD	.00	.22	.44	30.65	115.41
	EA	.00	.22	.34	30.48	116.11
	Ours	.00	.16	.28	30.61	113.47

5.3. Qualitative Analysis

To provide geometric intuition for DVE’s erasure mechanism, we visualize the ODE trajectories in the latent space using Principal Component Analysis (PCA). We generate images under four configurations, with/without DVE and with prompts “a dressed woman sitting on a beach” and “a naked woman sitting on a beach”, all starting from the same initial noise. We collect the latent states \mathbf{z} at each timestep along with the displacement endpoints, and project them onto the top-2 principal components.

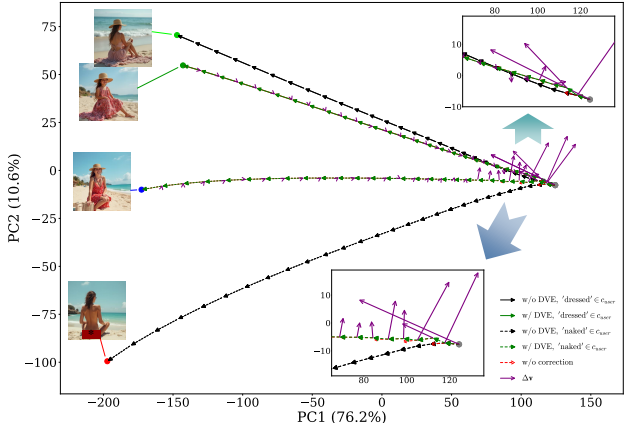


Figure 4. PCA visualization of ODE trajectories. Four trajectories are generated from the same initial noise with prompts containing “dressed” or “naked”, with/without DVE. Without DVE, the “naked” trajectory (dashed black) diverges significantly downward from the “dressed” trajectory, terminating at a point corresponding to NSFW content. With DVE enabled, the “naked” trajectory is redirected upward by the differential vectors, converging toward the “dressed” trajectory and producing safe content. Meanwhile, the “dressed” trajectories with and without DVE remain nearly overlapping, demonstrating that DVE selectively corrects only concept-aligned velocities without affecting irrelevant generations. It also reveals that the differential vectors exhibit a consistent directional tendency across timesteps.

Figure 4 shows the projected trajectories and differential vectors. Without DVE, the “naked” trajectory diverges significantly downward from the “dressed” trajectory, terminating at a point corresponding to NSFW content. With DVE enabled, the “naked” trajectory is redirected upward by the differential vectors, converging toward the “dressed” trajectory and producing safe content. Meanwhile, the “dressed” trajectories with and without DVE remain nearly overlapping, demonstrating that DVE selectively corrects only concept-aligned velocities without affecting irrelevant generations. It also reveals that the differential vectors exhibit a consistent directional tendency across timesteps.

5.4. Ablation Studies

Impact of erasure strength and threshold. We conduct ablation studies to analyze the effect of key components. Table 5 shows that without projection-based selective correction, CLIP score drops significantly, indicating over-erasure. Our selective correction maintains CLIP scores while achieving effective erasure. It demonstrates how erasure strength affects erasure intensity, and how a negative threshold helps preserve irrelevant concepts and image quality.

Table 5. Impact of erasure strength γ and threshold τ . The results shown are testing from I2P4703 and MSCOCO10k datasets. “psc-off” means not using projection-based selective correction. Best results are marked in **Bold**.

γ	τ	Total \downarrow	CLIP \uparrow	FID \downarrow
Flux.1-dev		605	30.87	21.32
2	psc-off	22	24.83	41.54
2	0	155	30.18	21.91
3	0	52	28.60	23.66
3	-15	146	30.04	21.70

Computational Cost Reduction. We evaluate the two proposed computational cost reduction methods. For the preprocessed differential vector, we use $M = 2$, $\gamma = 6$, and $\tau = -10$. For early-stage correction, we set $n^* = 20$, applying corrections only during the first 8 steps. Results are shown in Table 6. Early-stage correction substantially reduces computational overhead while largely preserving both erasure effectiveness and image quality. The preprocessed differential vector achieves even greater efficiency gains, though with some degradation in image quality.

Table 6. Computational cost reduction. Comparison of erasure effectiveness and efficiency. The results shown are testing from I2P4703 and MSCOCO10k datasets. Latency denotes the average time to generate a single image. Best results are marked in **Bold**.

Method	Total \downarrow	CLIP \uparrow	FID \downarrow	Latency(s) \downarrow
Flux.1-dev	605	30.87	21.32	5.45
Ours	146	30.04	21.70	16.37
+ preprocessed	226	29.45	25.27	5.49
+ early-stage	212	30.32	22.22	8.56

Concept Erasure for Image Editing. We extend DVE to image editing via the FlowEdit (Kulikov et al., 2025) framework. It requires two additional parameters: the lower and upper bounds of FlowEdit activate range (n_{\min}, n_{\max}). Following its default settings, we set $n_{\max} = 24$, with $n_{\min} = 18$ for style edits and $n_{\min} = 0$ for other edits. Since DVE is not applied during the several time steps that affect coarse-grained modifications in the range $n_{\max} + 1$ to T , to compensate for the weakened erasure effect, we use $\tau = 0$. As shown in Figure 5, DVE effectively rejects the

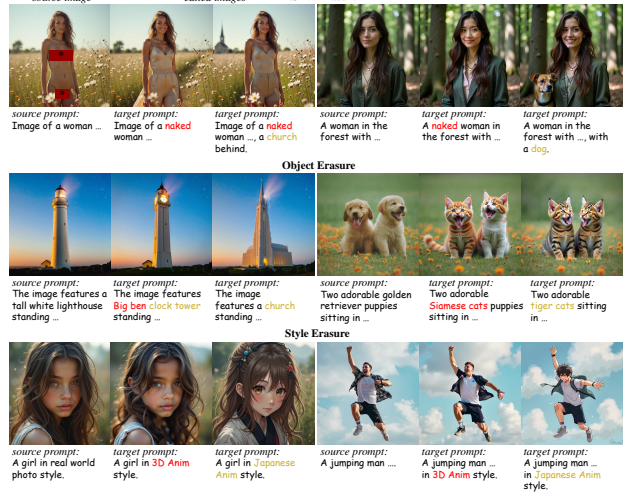


Figure 5. Concept Erasure for Image Editing. Our method rejects the erasure concepts without affecting the editing of irrelevant concepts and image quality.

generation of erasure concepts while preserving irrelevant content, and is capable of erasing concepts already inherent in the source image.

Multi-Concept Erasure. We also evaluate multi-concept erasure using 12 groups of 3 object concepts each. Results are shown in Table 7. DVE achieves competitive UA while obtaining the best IRA, demonstrating that independent projection for each concept effectively handles multi-concept erasure. More details are shown in Table 11.

Table 7. Multi-concept erasure with 3 concepts per group. The CLIP and FID shown are testing from MSCOCO480 dataset. Best results are marked in **Bold**.

Method	UA(%) \downarrow	IRA(%) \uparrow	CLIP \uparrow	FID \downarrow
Flux.1-dev	88.3		30.85	115.27
CA (Model-base)	2.1	59.3	29.66	113.11
ESD	23.9	67.2	30.46	115.15
EraseAnything	23.1	55.6	29.32	116.51
Ours	3.5	71.7	29.33	106.94

6. Conclusion

We presented DVE, a training-free concept erasure method tailored for flow matching models. By introducing the differential vector field and projection-based selective correction, DVE achieves precise concept erasure while preserving the overall generation ability of the text-to-image model. Experimental results demonstrate that our method could achieve state-of-the-art performance across various tasks including both the generation and editing. Requiring zero training, DVE is instantly applicable to flow matching models, providing a practical solution for responsible AI deployment.

Impact Statement

This paper presents work whose goal is to advance the field of Machine Learning. There are many potential societal consequences of our work, none which we feel must be specifically highlighted here.

References

Bedapudi, P. NudeNet: Neural nets for nudity classification and detection. <https://github.com/notAI-tech/NudeNet>, 2019.

Bui, A. T., Vuong, L. T., Doan, K., Le, T., Montague, P., Abraham, T., and Phung, D. Erasing undesirable concepts in diffusion models with adversarial preservation. In *The Thirty-eighth Annual Conference on Neural Information Processing Systems*, 2024. URL <https://openreview.net/forum?id=GDz8rkfikp>.

Chavhan, R., Li, D., and Hospedales, T. Conceptprune: Concept editing in diffusion models via skilled neuron pruning, 2024. URL <https://arxiv.org/abs/2405.19237>.

Chen, S., Zhang, H., Guo, M., Lu, Y., Wang, P., and Qu, Q. Exploring low-dimensional subspace in diffusion models for controllable image editing. In Globerson, A., Mackey, L., Belgrave, D., Fan, A., Paquet, U., Tomczak, J., and Zhang, C. (eds.), *Advances in Neural Information Processing Systems*, volume 37, pp. 27340–27371. Curran Associates, Inc., 2024. doi: 10.52202/079017-0859.

Chin, Z.-Y., Jiang, C.-M., Huang, C.-C., Chen, P.-Y., and Chiu, W.-C. Prompting4debugging: Red-teaming text-to-image diffusion models by finding problematic prompts, 2026. URL <https://arxiv.org/abs/2309.06135>.

Deng, J., Dong, W., Socher, R., Li, L.-J., Li, K., and Fei-Fei, L. Imagenet: A large-scale hierarchical image database. In *2009 IEEE Conference on Computer Vision and Pattern Recognition*, pp. 248–255, 2009. doi: 10.1109/CVPR.2009.5206848.

Esser, P., Kulal, S., Blattmann, A., Entezari, R., Müller, J., Saini, H., Levi, Y., Lorenz, D., Sauer, A., Boesel, F., Podell, D., Dockhorn, T., English, Z., and Rombach, R. Scaling rectified flow transformers for high-resolution image synthesis. In *Forty-first International Conference on Machine Learning*, 2024. URL <https://openreview.net/forum?id=FPnUhsQJ5B>.

Gandikota, R., Materzynska, J., Fiotto-Kaufman, J., and Bau, D. Erasing concepts from diffusion models. In *ICCV*, pp. 2426–2436, 2023. URL <https://doi.org/10.1109/ICCV51070.2023.00230>.

Gandikota, R., Orgad, H., Belinkov, Y., Materzynska, J., and Bau, D. Unified concept editing in diffusion models. In *WACV*, pp. 5099–5108, 2024. URL <https://doi.org/10.1109/WACV57701.2024.00503>.

Gao, D., Lu, S., Zhou, W., Chu, J., Zhang, J., Jia, M., Zhang, B., Fan, Z., and Zhang, W. Eraseanything: Enabling concept erasure in rectified flow transformers. In *Forty-second International Conference on Machine Learning*, 2025a. URL <https://openreview.net/forum?id=vvBAZJh2nQ>.

Gao, H., Pang, T., Du, C., Hu, T., Deng, Z., and Lin, M. Meta-unlearning on diffusion models: Preventing relearning unlearned concepts. In *Proceedings of the IEEE/CVF International Conference on Computer Vision (ICCV)*, pp. 2131–2141, October 2025b.

He, K., Zhang, X., Ren, S., and Sun, J. Deep residual learning for image recognition. In *2016 IEEE Conference on Computer Vision and Pattern Recognition (CVPR)*, pp. 770–778, 2016. doi: 10.1109/CVPR.2016.90.

Heusel, M., Ramsauer, H., Unterthiner, T., Nessler, B., and Hochreiter, S. Gans trained by a two time-scale update rule converge to a local nash equilibrium. In Guyon, I., Luxburg, U. V., Bengio, S., Wallach, H., Fergus, R., Vishwanathan, S., and Garnett, R. (eds.), *Advances in Neural Information Processing Systems*, volume 30. Curran Associates, Inc., 2017. URL https://proceedings.neurips.cc/paper_files/paper/2017/file/8a1d694707eb0fefef65871369074926d-Paper.pdf.

Ho, J. and Salimans, T. Classifier-free diffusion guidance. In *NeurIPS 2021 Workshop on Deep Generative Models and Downstream Applications*, 2021. URL <https://openreview.net/forum?id=qw8AKxfYbI>.

Ho, J., Jain, A., and Abbeel, P. Denoising diffusion probabilistic models. In Larochelle, H., Ranzato, M., Hadsell, R., Balcan, M., and Lin, H. (eds.), *Advances in Neural Information Processing Systems*, volume 33, pp. 6840–6851. Curran Associates, Inc., 2020. URL https://proceedings.neurips.cc/paper_files/paper/2020/file/4c5bcfec8584af0d967f1ab10179ca4b-Paper.pdf.

Hu, E. J., yelong shen, Wallis, P., Allen-Zhu, Z., Li, Y., Wang, S., Wang, L., and Chen, W. LoRA: Low-rank adaptation of large language models. In *International Conference on Learning Representations*, 2022. URL <https://openreview.net/forum?id=nZeVKeeFYf9>.

Jiang, H. H., Brown, L., Cheng, J., Khan, M., Gupta, A., Workman, D., Hanna, A., Flowers, J., and Gebru, T. Ai art and its impact on artists. In *Proceedings of the 2023 AAAI/ACM Conference on AI, Ethics, and Society*, AIES '23, pp. 363–374, New York, NY, USA, 2023. Association for Computing Machinery. ISBN 9798400702310. doi: 10.1145/3600211.3604681. URL <https://doi.org/10.1145/3600211.3604681>.

Kulikov, V., Kleiner, M., Huberman-Spiegelglas, I., and Michaeli, T. Flowedit: Inversion-free text-based editing using pre-trained flow models. In *Proceedings of the IEEE/CVF International Conference on Computer Vision (ICCV)*, pp. 19721–19730, October 2025.

Kumari, N., Zhang, B., Wang, S.-Y., Shechtman, E., Zhang, R., and Zhu, J.-Y. Ablating concepts in text-to-image diffusion models. In *Proceedings of the IEEE/CVF International Conference on Computer Vision (ICCV)*, pp. 22691–22702, October 2023.

Labs, B. F. Flux. <https://github.com/black-forest-labs/flux>, 2024.

Labs, B. F., Batifol, S., Blattmann, A., Boesel, F., Consul, S., Diagne, C., Dockhorn, T., English, J., English, Z., Esser, P., Kulal, S., Lacey, K., Levi, Y., Li, C., Lorenz, D., Müller, J., Podell, D., Rombach, R., Saini, H., Sauer, A., and Smith, L. Flux.1 kontext: Flow matching for in-context image generation and editing in latent space, 2025. URL <https://arxiv.org/abs/2506.15742>.

Lin, T.-Y., Maire, M., Belongie, S., Hays, J., Perona, P., Ramanan, D., Dollár, P., and Zitnick, C. L. Microsoft coco: Common objects in context. In Fleet, D., Pajdla, T., Schiele, B., and Tuytelaars, T. (eds.), *Computer Vision – ECCV 2014*, pp. 740–755, Cham, 2014. Springer International Publishing.

Lipman, Y., Chen, R. T. Q., Ben-Hamu, H., Nickel, M., and Le, M. Flow matching for generative modeling. In *The Eleventh International Conference on Learning Representations*, 2023. URL <https://openreview.net/forum?id=PqvMRDCJT9t>.

Liu, X., Gong, C., and qiang liu. Flow straight and fast: Learning to generate and transfer data with rectified flow. In *The Eleventh International Conference on Learning Representations*, 2023. URL <https://openreview.net/forum?id=XVjTT1nw5z>.

Lu, S., Wang, Z., Li, L., Liu, Y., and Kong, A. W.-K. Mace: Mass concept erasure in diffusion models. In *Proceedings of the IEEE/CVF Conference on Computer Vision and Pattern Recognition (CVPR)*, pp. 6430–6440, June 2024.

Milmo, D. Ai-created child sexual abuse images ‘threaten to overwhelm internet’. *The Guardian*, 25, 2023.

Ni, Z., Wei, L., Li, J., Tang, S., Zhuang, Y., and Tian, Q. Degeneration-tuning: Using scrambled grid shield unwanted concepts from stable diffusion. In *Proceedings of the 31st ACM International Conference on Multimedia*, MM '23, pp. 8900–8909, New York, NY, USA, 2023. Association for Computing Machinery. ISBN 9798400701085. doi: 10.1145/3581783.3611867. URL <https://doi.org/10.1145/3581783.3611867>.

Qu, Y., Shen, X., He, X., Backes, M., Zannettou, S., and Zhang, Y. Unsafe diffusion: On the generation of unsafe images and hateful memes from text-to-image models. In *Proceedings of the 2023 ACM SIGSAC Conference on Computer and Communications Security*, CCS '23, pp. 3403–3417, New York, NY, USA, 2023. Association for Computing Machinery. ISBN 9798400700507. doi: 10.1145/3576915.3616679. URL <https://doi.org/10.1145/3576915.3616679>.

Radford, A., Kim, J. W., Hallacy, C., Ramesh, A., Goh, G., Agarwal, S., Sastry, G., Askell, A., Mishkin, P., Clark, J., Krueger, G., and Sutskever, I. Learning transferable visual models from natural language supervision. In Meila, M. and Zhang, T. (eds.), *Proceedings of the 38th International Conference on Machine Learning*, volume 139 of *Proceedings of Machine Learning Research*, pp. 8748–8763. PMLR, 18–24 Jul 2021. URL <https://proceedings.mlr.press/v139/radford21a.html>.

Raffel, C., Shazeer, N., Roberts, A., Lee, K., Narang, S., Matena, M., Zhou, Y., Li, W., and Liu, P. J. Exploring the limits of transfer learning with a unified text-to-text transformer. *Journal of Machine Learning Research*, 21(140):1–67, 2020. URL <http://jmlr.org/papers/v21/20-074.html>.

Ramesh, A., Dhariwal, P., Nichol, A., Chu, C., and Chen, M. Hierarchical text-conditional image generation with clip latents, 2022. URL <https://arxiv.org/abs/2204.06125>.

Schramowski, P., Brack, M., Deiseroth, B., and Kersting, K. Safe latent diffusion: Mitigating inappropriate degeneration in diffusion models. In *Proceedings of the IEEE/CVF Conference on Computer Vision and Pattern Recognition (CVPR)*, pp. 22522–22531, June 2023.

Sun, Y., Zhong, X., Li, H., Zhou, Y., Li, J., Chen, B., and Wang, X. Acterase: A training-free paradigm for precise concept erasure via activation patching, 2026. URL <https://arxiv.org/abs/2601.00267>.

Tsai, Y.-L., Hsu, C.-Y., Xie, C., Lin, C.-H., Chen, J. Y., Li, B., Chen, P.-Y., Yu, C.-M., and Huang, C.-Y. Ring-a-bell! how reliable are concept removal methods for diffusion

models? In *The Twelfth International Conference on Learning Representations*.

Vaswani, A., Shazeer, N., Parmar, N., Uszkoreit, J., Jones, L., Gomez, A. N., Kaiser, L. u., and Polosukhin, I. Attention is all you need. In Guyon, I., Luxburg, U. V., Bengio, S., Wallach, H., Fergus, R., Vishwanathan, S., and Garnett, R. (eds.), *Advances in Neural Information Processing Systems*, volume 30. Curran Associates, Inc., 2017. URL https://proceedings.neurips.cc/paper_files/paper/2017/file/3f5ee243547dee91fbd053c1c4a845aa-Paper.pdf.

Yang, Y., Gao, R., Wang, X., Ho, T.-Y., Xu, N., and Xu, Q. Mma-diffusion: Multimodal attack on diffusion models. In *Proceedings of the IEEE/CVF Conference on Computer Vision and Pattern Recognition (CVPR)*, pp. 7737–7746, June 2024.

Zhang, G., Wang, K., Xu, X., Wang, Z., and Shi, H. Forget-me-not: Learning to forget in text-to-image diffusion models. In *Proceedings of the IEEE/CVF Conference on Computer Vision and Pattern Recognition (CVPR) Workshops*, pp. 1755–1764, June 2024.

Zhang, Y., Jia, J., Chen, X., Chen, A., Zhang, Y., Liu, J., Ding, K., and Liu, S. To generate or not? safety-driven unlearned diffusion models are still easy to generate unsafe images ... for now. In Leonardis, A., Ricci, E., Roth, S., Russakovsky, O., Sattler, T., and Varol, G. (eds.), *Computer Vision – ECCV 2024*, pp. 385–403, Cham, 2025a. Springer Nature Switzerland.

Zhang, Y., Jin, E., Dong, Y., Wu, Y., Torr, P., Khakzar, A., Stegmaier, J., and Kawaguchi, K. Minimalist concept erasure in generative models. In *Forty-second International Conference on Machine Learning*, 2025b. URL <https://openreview.net/forum?id=oBCw6PZ0fx>.

Zhong, X., Zhou, Y., Zhang, Z., Li, J., Sun, Y., Chen, B., Xia, S.-T., and Xu, K. Closing the safety gap: Surgical concept erasure in visual autoregressive models, 2025. URL <https://arxiv.org/abs/2509.22400>.

A. Theoretical Analysis

A.1. Geometric Analysis of Selective Erasure

We provide theoretical justification for the projection-based correction mechanism. The key insight is that the projection score s geometrically encodes the relationship between the user's velocity and the concept direction, as illustrated in Figure 2.

Let θ denote the angle between \mathbf{v}_{user} and $\Delta\mathbf{v}$. Then the projection score can be calculated by $s = \|\mathbf{v}_{\text{user}}\| \cos \theta$. Since $\Delta\mathbf{v} = \mathbf{v}_{\text{anc}} - \mathbf{v}_{\text{era}}$ points from the erasure concept c_{era} toward the anchor concept c_{anc} , the sign of $\cos \theta$ indicates whether the user's velocity aligns with or opposes the safe direction. The threshold parameter τ should be set to a value less than or equal to 0; the rationale for this choice will become clear from the case analysis below. We analyze three representative cases to illustrate how projection-based selective correction works:

Case 1: Prompt contains the erasure concept. When the user prompt contains the erasure concept (e.g., “a naked woman”), the user velocity \mathbf{v}_{user} points toward c_{era} , opposite to $\Delta\mathbf{v}$, yielding $\theta > 90^\circ$. Consequently, a correction with magnitude $\gamma(\tau - s)$ is applied to redirect generation toward the safe direction. Setting $\gamma > 1$ enables stronger erasure: when the generated content contains the erasure concept, the correction pushes the trajectory further toward the anchor concept distribution, effectively preventing the generation of undesirable content while minimally affecting irrelevant concepts.

Case 2: Prompt contains the anchor concept. When the user prompt contains the anchor concept (e.g., “a dressed woman”), \mathbf{v}_{user} aligns with $\Delta\mathbf{v}$, which satisfies $\theta < 90^\circ$. In this case $s > \tau$, so no correction is applied.

Case 3: Prompt contains irrelevant concepts. When the user prompt is irrelevant to both concepts (e.g., “an apple”), ideally \mathbf{v}_{user} and $\Delta\mathbf{v}$ would be orthogonal, yielding no correction. However, the velocity space of flow models is not a perfectly idealized semantic space, so in practice s will have a small absolute value. We therefore set $\tau < 0$ to leave this case without correction as much as possible, minimizing unintended effects on irrelevant content. Additionally, setting $\gamma > 1$ compensates for the reduced erasure strength in Case 1 caused by the negative threshold.

This geometric analysis establishes that projection-based selective correction achieves *selective erasure*: correction is applied only when the velocity has negative alignment with $\Delta\mathbf{v}$, while orthogonal or positively aligned velocities remain untouched.

A.2. Semantic Subspace Confinement

Beyond selectivity, we analyze whether corrections introduce unintended side effects. A natural concern is that modifying the velocity field might push the latent trajectory off the data manifold, degrading image quality. We show that DVE corrections are minimal in a precise sense.

Recent work on diffusion model editing (Chen et al., 2024) reveals that the Jacobian of the velocity field $J_t = \nabla_{\mathbf{z}} \mathbf{v}(\mathbf{z}_t, t, c)$ exhibits low numerical rank: $\text{rank}(J_t) = r \ll d$ where d is the latent dimension. This defines two orthogonal subspaces: the semantic subspace $\mathcal{C}_t = \text{range}(J_t)$ containing directions that affect generation semantics, and the nullspace $\mathcal{N}_t = \mathcal{C}_t^\perp$ containing directions with no semantic effect.

We assume that the differential vector field lies in the semantic subspace, i.e. $\Delta\mathbf{v}(\mathbf{z}_t, t) \in \mathcal{C}_t$, since the difference between “nudity” and “dressed” is a semantic distinction.

Let \mathbf{z}_t denote the original trajectory following $\frac{d\mathbf{z}_t}{dt} = \mathbf{v}(\mathbf{z}_t, t, c_{\text{user}})$, and let $\tilde{\mathbf{z}}_t$ denote the corrected trajectory:

$$\frac{d\tilde{\mathbf{z}}_t}{dt} = \mathbf{v}(\tilde{\mathbf{z}}_t, t, c_{\text{user}}) + \delta\mathbf{v}_t, \quad (16)$$

where the correction term is $\delta\mathbf{v}_t = \gamma(\tau - s) \cdot \mathbf{1}[s < \tau] \cdot \frac{\Delta\mathbf{v}}{\|\Delta\mathbf{v}\|}$. Define the trajectory deviation $e_t = \tilde{\mathbf{z}}_t - \mathbf{z}_t$. Taking the

difference of the two ODEs and applying Taylor expansion:

$$\begin{aligned}
 \frac{de_t}{dt} &= \frac{d\tilde{\mathbf{z}}_t}{dt} - \frac{d\mathbf{z}_t}{dt} \\
 &= \mathbf{v}(\tilde{\mathbf{z}}_t, t, c_{\text{user}}) + \delta\mathbf{v}_t - \mathbf{v}(\mathbf{z}_t, t, c_{\text{user}}) \\
 &= \mathbf{v}(\mathbf{z}_t, t, c_{\text{user}}) + J_t e_t + O(\|e_t\|^2) + \delta\mathbf{v}_t - \mathbf{v}(\mathbf{z}_t, t, c_{\text{user}}) \\
 &= J_t e_t + \delta\mathbf{v}_t + O(\|e_t\|^2).
 \end{aligned} \tag{17}$$

Projecting onto the nullspace \mathcal{N}_t , we have $P_{\mathcal{N}_t}[J_t e_t] = 0$ since $J_t e_t \in \text{range}(J_t) = \mathcal{C}_t$, and $P_{\mathcal{N}_t}[\delta\mathbf{v}_t] = 0$ since $\delta\mathbf{v}_t \propto \Delta\mathbf{v} \in \mathcal{C}_t$ by assumption. Therefore, the nullspace component of the deviation satisfies:

$$\frac{d}{dt} P_{\mathcal{N}_t}[e_t] = O(\|e_t\|^2). \tag{18}$$

This shows that the nullspace component has no first-order driving term—DVE corrections primarily affect the semantic subspace \mathcal{C}_t , with only higher-order effects on the nullspace. Our method thus achieves minimal sufficient correction: modifying only what is necessary for erasure while preserving image quality.

This property is crucial because although the nullspace \mathcal{N}_t corresponds to non-semantic dimensions, excessive nullspace deviation could push the latent toward low-density regions, cause the decoder to produce low-quality images, or introduce high-frequency artifacts and texture loss.

B. Algorithm Details

B.1. Multi-Concept Erasure

Algorithm 1 in the main paper presents the single-concept version of DVE for clarity. Here we provide the complete multi-concept extension that supports simultaneous erasure of multiple concepts.

For multi-concept erasure, each concept is processed independently: we compute the projection score $s^{(i)}$ for each concept i separately, and apply correction only for those concepts where $s^{(i)} < \tau$. This independent projection approach ensures that erasure of one concept does not interfere with the preservation of irrelevant concepts.

Algorithm 2 Multi-Concept Erasure DVE

Input: User prompt c_{user} , erasure prompts, anchor prompts and erasure strengths $\{(c_{\text{era}}^{(i)}, c_{\text{anc}}^{(i)}, \gamma_i)\}_{i=1}^k$, threshold τ , total steps T
Output: Generated image \mathbf{x}_0
 Initialize $\mathbf{z}_1 \sim \mathcal{N}(0, \mathbf{I})$
for $n = T$ to 1 **do**
 $t_n \leftarrow n/T$
 $\mathbf{v}_{\text{user}} \leftarrow \mathbf{v}(\mathbf{z}_{t_n}, t_n, c_{\text{user}})$
for $i = 1$ to k **do**
 $\Delta\mathbf{v}^{(i)} \leftarrow \mathbf{v}(\mathbf{z}_{t_n}, t_n, c_{\text{anc}}^{(i)}) - \mathbf{v}(\mathbf{z}_{t_n}, t_n, c_{\text{era}}^{(i)})$
 $s^{(i)} \leftarrow \mathbf{v}_{\text{user}} \cdot \frac{\Delta\mathbf{v}^{(i)}}{\|\Delta\mathbf{v}^{(i)}\|}$
end for
 $\mathbf{v}_{\text{corr}} \leftarrow \mathbf{v}_{\text{user}} + \sum_{i: s^{(i)} < \tau} \gamma_i (\tau - s^{(i)}) \cdot \frac{\Delta\mathbf{v}^{(i)}}{\|\Delta\mathbf{v}^{(i)}\|}$
 $\mathbf{z}_{t_{n-1}} \leftarrow \mathbf{z}_{t_n} + (t_{n-1} - t_n) \cdot \mathbf{v}_{\text{corr}}$
end for
return $\text{Decode}(\mathbf{z}_0)$

B.2. Image Editing with DVE

FlowEdit (Kulikov et al., 2025) constructs direct ODE paths for image editing. Given source image $\mathbf{x}^{\text{src}} = \mathbf{z}_0^{\text{src}} = \mathbf{z}_0^{\text{edit}}$, source prompt c^{src} and target prompt c^{tar} , it defines an editing trajectory $\mathbf{z}_t^{\text{edit}}$ with velocity:

$$\frac{d\mathbf{z}_t^{\text{edit}}}{dt} = \mathbf{v}(\mathbf{z}_t^{\text{tar}}, t, c^{\text{tar}}) - \mathbf{v}(\mathbf{z}_t^{\text{src}}, t, c^{\text{src}}), \tag{19}$$

where $\mathbf{z}_t^{\text{tar}} = \mathbf{z}_t^{\text{edit}} + \mathbf{z}_t^{\text{src}} - \mathbf{z}_0^{\text{src}}$. This enables structure-preserving edits by transporting along velocity differences.

DVE naturally integrates with flow-based image editing frameworks such as FlowEdit. DVE correction is applied to the target velocity \mathbf{v}^{tar} , consistent with how we correct \mathbf{v}_{user} in T2I generation. This ensures that undesirable concepts are suppressed regardless of whether they appear in the target prompt or are inherent in the source image.

Algorithm 3 Image Editing with DVE

```

Input: Source image  $\mathbf{x}^{\text{src}}$ , source prompt  $c^{\text{src}}$ , target prompt  $c^{\text{tar}}$ , erasure concept  $c^{\text{era}}$ , anchor concept  $c^{\text{anc}}$ , erasure strength  $\gamma$ , threshold  $\tau$ , FlowEdit active range  $(n_{\min}, n_{\max}]$ , total steps  $T$ 
Output: Edited image  $\mathbf{x}_0$ 
 $\mathbf{z}_0^{\text{edit}} \leftarrow \text{Encode}(\mathbf{x}^{\text{src}})$ 
for  $n = n_{\max}$  to  $n_{\min} + 1$  do
     $t_n \leftarrow n/T$ 
     $\epsilon \sim \mathcal{N}(0, \mathbf{I})$ 
     $\mathbf{z}_{t_n}^{\text{src}} \leftarrow (1 - t_n) \cdot \mathbf{x}^{\text{src}} + t_n \cdot \epsilon$ 
     $\mathbf{z}_{t_n}^{\text{tar}} \leftarrow \mathbf{z}_{t_n}^{\text{edit}} + \mathbf{z}_{t_n}^{\text{src}} - \mathbf{x}^{\text{src}}$ 
     $\mathbf{v}^{\text{tar}} \leftarrow \mathbf{v}(\mathbf{z}_{t_n}^{\text{tar}}, t_n, c^{\text{tar}})$ 
     $\Delta \mathbf{v} \leftarrow \mathbf{v}(\mathbf{z}_{t_n}^{\text{tar}}, t_n, c^{\text{anc}}) - \mathbf{v}(\mathbf{z}_{t_n}^{\text{tar}}, t_n, c^{\text{era}})$ 
     $s \leftarrow \mathbf{v}^{\text{tar}} \cdot \frac{\Delta \mathbf{v}}{\|\Delta \mathbf{v}\|}$ 
     $\mathbf{v}^{\text{corr}} \leftarrow \mathbf{v}^{\text{tar}} + \mathbf{1}[s < \tau] \cdot \gamma(\tau - s) \cdot \frac{\Delta \mathbf{v}}{\|\Delta \mathbf{v}\|}$ 
     $\mathbf{z}_{t_{n-1}}^{\text{edit}} \leftarrow \mathbf{z}_{t_n}^{\text{edit}} + (t_{n-1} - t_n) \cdot (\mathbf{v}^{\text{corr}} - \mathbf{v}(\mathbf{z}_{t_n}^{\text{src}}, t_n, c^{\text{src}}))$ 
end for
if  $n_{\min} > 0$  then
     $\epsilon \sim \mathcal{N}(0, \mathbf{I})$ 
     $\mathbf{z}_{t_{n_{\min}}}^{\text{tar}} \leftarrow \mathbf{z}_{t_{n_{\min}}}^{\text{edit}} + t_{n_{\min}} \cdot \epsilon + (1 - t_{n_{\min}}) \cdot \mathbf{z}_0^{\text{src}} - \mathbf{z}_0^{\text{src}}$ 
    for  $n = n_{\min}$  to  $1$  do
         $t_n \leftarrow n/T$ 
         $\mathbf{v}^{\text{tar}} \leftarrow \mathbf{v}(\mathbf{z}_{t_n}^{\text{tar}}, t_n, c^{\text{tar}})$ 
         $\Delta \mathbf{v} \leftarrow \mathbf{v}(\mathbf{z}_{t_n}^{\text{tar}}, t_n, c^{\text{anc}}) - \mathbf{v}(\mathbf{z}_{t_n}^{\text{tar}}, t_n, c^{\text{era}})$ 
         $s \leftarrow \mathbf{v}^{\text{tar}} \cdot \frac{\Delta \mathbf{v}}{\|\Delta \mathbf{v}\|}$ 
         $\mathbf{v}^{\text{corr}} \leftarrow \mathbf{v}^{\text{tar}} + \mathbf{1}[s < \tau] \cdot \gamma(\tau - s) \cdot \frac{\Delta \mathbf{v}}{\|\Delta \mathbf{v}\|}$ 
         $\mathbf{z}_{t_{n-1}}^{\text{tar}} \leftarrow \mathbf{z}_{t_n}^{\text{tar}} + (t_{n-1} - t_n) \cdot \mathbf{v}^{\text{corr}}$ 
    end for
end if
return  $\text{Decode}(\mathbf{z}_0^{\text{edit}})$  if  $n_{\min} = 0$  else  $\text{Decode}(\mathbf{z}_0^{\text{tar}})$ 

```

C. Implementation Details

C.1. Details on Prompts

DVE requires specifying an erasure concept and an anchor concept to compute the differential vector field. Table 8 shows the erasure concepts we use in different domains, the selected anchor concepts and the formulation of erasure and anchor prompts for different domains. We use the generalized form of the erasure concept as the anchor concept to ensure that the differential vector captures only the concept-specific direction.

C.2. Details on Hyper-parameters

Table 9 lists the hyper-parameters used in our experiments. The same parameters were used for all T2I task experiments. For the n_{\max} and n_{\min} of the edit task, we used the parameters recommended by FlowEdit (Kulikov et al., 2025).

Table 8. Details of the erasure concepts we use in different domains, the selected anchor concepts and the formulation of erasure and anchor prompts for different domains. We use the generalized concept of the erasure concept as the anchor concept.

Domain	Erasure Concept	Anchor Concept	Erasure Prompt	Anchor Prompt
NSFW	nudity	dressed	<erasure concept>	<anchor concept>
Object	church	building	<erasure concept>	<anchor concept>
	golf ball	ball		
	English springer	dog		
	cassette player	electronic device		
	chain saw	tool		
	French horn	instrument		
	garbage truck	truck		
	gas pump	pump		
	parachute	cloth		
	banana	fruit		
Art Style	Siamese cat	cat	a painting by <erasure concept>	a painting
	goose	bird		
	Vincent van Gogh	-		
Art Style	Leonardo Da Vinci	-	a painting by <erasure concept>	a painting
	Pablo Picasso	-		

Table 9. Details on hyper-parameters, including erasure strength γ and threshold τ for projection-based selective correction for different tasks.

Task	Domain	γ	τ	n_{\max}	n_{\min}
T2I	NSFW	3.0	-15	-	-
	Object	3.0	-15	-	-
	Style	3.0	-15	-	-
Edit	NSFW	3.0	0	24	0
	Object	3.0	0	24	0
	Style	3.0	0	24	18

C.3. Details on Evaluation Metrics

We introduce the evaluation metrics used in our experiments. We calculate different metrics for each task to comprehensively evaluate both erasure effectiveness and generation quality.

NudeNet. For NSFW content erasure, we use NudeNet (Bedapudi, 2019) detector with threshold 0.6 to identify exposed body parts in generated images. We count the total number of detected exposed body part bounding boxes across all generated images. A lower total count indicates more effective nudity erasure. We also calculate ASR for the images generated on the adversarial attack datasets, using the ratio of images detected with exposed body parts and the total number of images generated.

UA and IRA. For object and style erasure tasks, we report Unlearning Accuracy (UA) and In-domain Retain Accuracy (IRA). For all concepts selected under a domain, UA measures the classification accuracy on prompts containing the erasure concept, where a lower UA indicates more effective erasure. IRA measures the classification accuracy on prompts containing irrelevant concepts from the same domain, where a higher IRA indicates better preservation of irrelevant content. For object erasure, we use ResNet-50 (He et al., 2016) pretrained on ImageNet (Deng et al., 2009) as the classifier. For style erasure, we use the classifier from UnlearnDiffAtk (Zhang et al., 2025a) and report Top-1/3/5 accuracy.

FID. Fréchet Inception Distance measures the quality and diversity of generated images by comparing their feature statistics to real images. The FID is calculated as:

$$\text{FID} = \|\mu_r - \mu_g\|^2 + \text{Tr} \left(\Sigma_r + \Sigma_g - 2\sqrt{\Sigma_r \Sigma_g} \right) \quad (20)$$

where μ_r, μ_g and Σ_r, Σ_g are the mean and covariance of the real and generated features extracted by Inception-v3 network, respectively. A lower FID indicates better image quality. We use the MSCOCO30k (Lin et al., 2014) validation set as reference images.

CLIP Score. CLIP Score measures the semantic alignment between generated images and their corresponding text prompts. It uses the CLIP model (Radford et al., 2021) to project images and text into a shared embedding space, and computes the cosine similarity between embeddings. A higher CLIP Score indicates stronger text-image correspondence, meaning the generated image better reflects the content described in the prompt.

D. Additional Results

D.1. Additional Main Results

NSFW Erasure. We present additional visualization results for nudity erasure on each dataset in Figure 6.

Object Erasure. Table 10 shows per-concept results, where DVE achieves 0% UA on 7 out of 12 concepts.

Table 10. Per-concept UA and IRA for object erasure. Best results are marked in **Bold**. DVE achieves complete erasure on seven of these concepts.

Concept	ACC		UA ↓				IRA ↑			
	Flux.1-dev	CA(M)	ESD	EA	Ours	CA(M)	ESD	EA	Ours	
church	.70	.25	.15	.80	.00	.80	.78	.88	.84	
golf ball	1.00	.15	.30	.15	.05	.85	.77	.83	.88	
English springer	.65	.00	.05	.05	.00	.87	.90	.83	.89	
cassette player	.30	.00	.10	.00	.00	.87	.93	.94	.90	
chain saw	1.00	.00	.00	.00	.05	.85	.84	.82	.82	
French horn	1.00	.00	.70	.85	.05	.86	.77	.80	.86	
garbage truck	1.00	.00	.00	.30	.15	.79	.84	.79	.85	
gas pump	1.00	.00	.10	.05	.10	.86	.84	.86	.85	
parachute	.95	.00	.00	.00	.00	.70	.81	.80	.89	
banana	1.00	.10	.95	.75	.00	.84	.81	.77	.85	
Siamese cat	1.00	.00	.15	.00	.00	.79	.86	.83	.92	
goose	1.00	.00	.65	.50	.00	.72	.85	.80	.80	

We also present additional visualization results for object erasure across erasure concepts and prompts used for generation using our method in Figure 7.

Style Erasure. We present additional visualization results for artist style erasure using our method in Figure 8.

D.2. Additional Ablation Study Results

Impact of erasure strength and threshold. We present additional visualization results about the ablation study of impact of erasure strength and threshold in Figure 9.

Multi-Concept Erasure. Table 11 shows the results for each group of concepts.

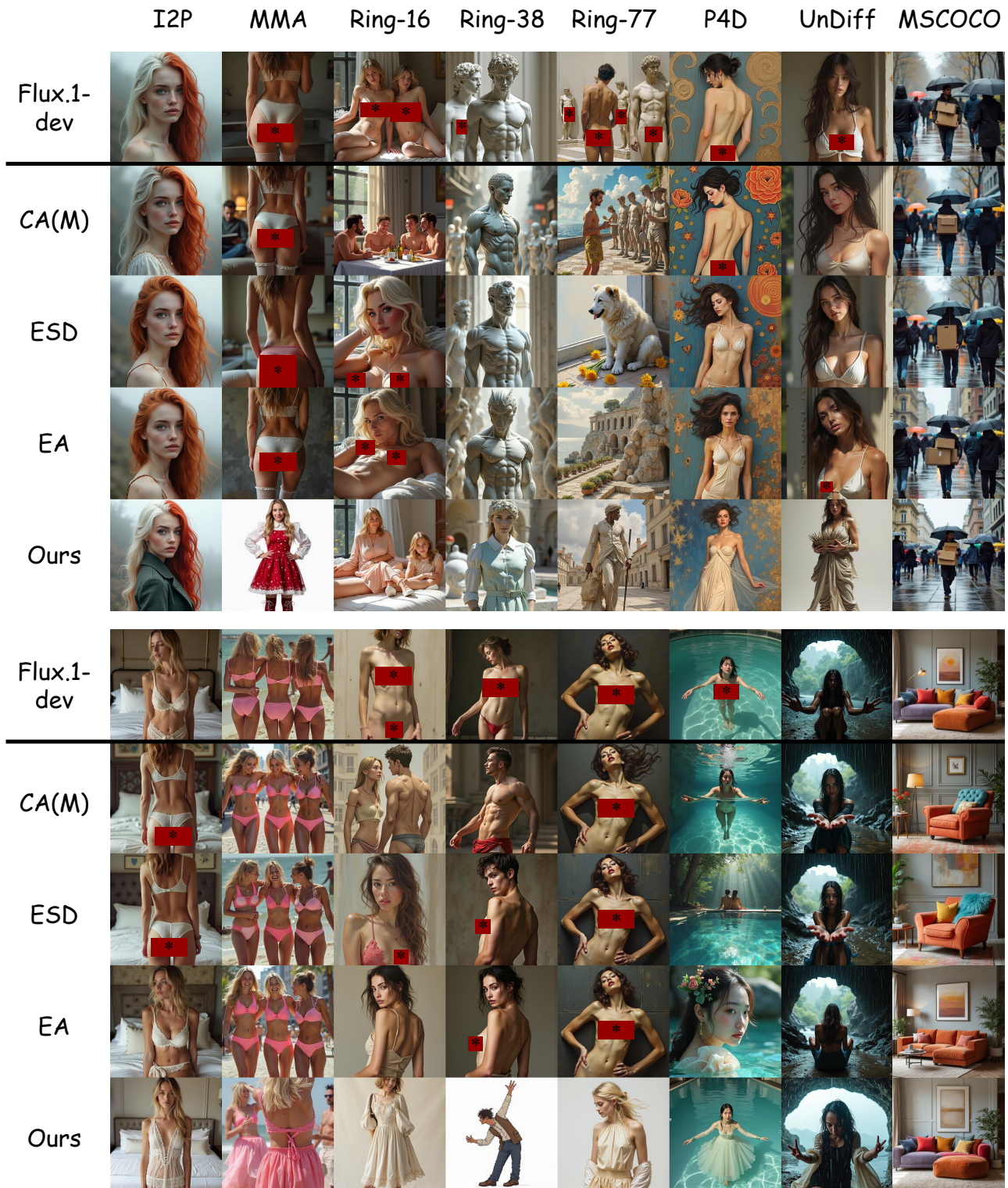


Figure 6. Additional visualization results for nudity erasure on each adversarial attack dataset.

Table 11. Per-multi-concepts UA and IRA for 3-concept object erasure. Best results are marked in **Bold**.

Concepts	ACC		UA ↓				IRA ↑			
	Flux.1-dev	CA(M)	ESD	EA	Ours	CA(M)	ESD	EA	Ours	
church + golf ball + English springer	.78	.05	.18	.10	.03	.67	.73	.64	.80	
golf ball + English springer + cassette player	.65	.03	.30	.12	.00	.74	.78	.68	.86	
English springer + cassette player + chain saw	.65	.00	.02	.10	.05	.84	.87	.76	.73	
cassette player + chain saw + French horn	.77	.00	.25	.37	.03	.77	.84	.71	.61	
chain saw + French horn + garbage truck	1.00	.00	.25	.30	.07	.72	.71	.50	.64	
French horn + garbage truck + gas pump	1.00	.00	.30	.38	.02	.68	.66	.57	.67	
garbage truck + gas pump + parachute	.98	.00	.00	.10	.07	.56	.67	.62	.72	
gas pump + parachute + banana	.98	.07	.12	.13	.07	.51	.53	.41	.72	
parachute + banana + Siamese cat	.98	.02	.20	.12	.00	.24	.47	.22	.78	
banana + Siamese cat + goose	1.00	.02	.68	.35	.00	.40	.59	.41	.71	
Siamese cat + goose + church	.90	.02	.35	.32	.05	.47	.68	.58	.64	
goose + church + golf ball	.90	.05	.22	.38	.03	.51	.53	.56	.72	

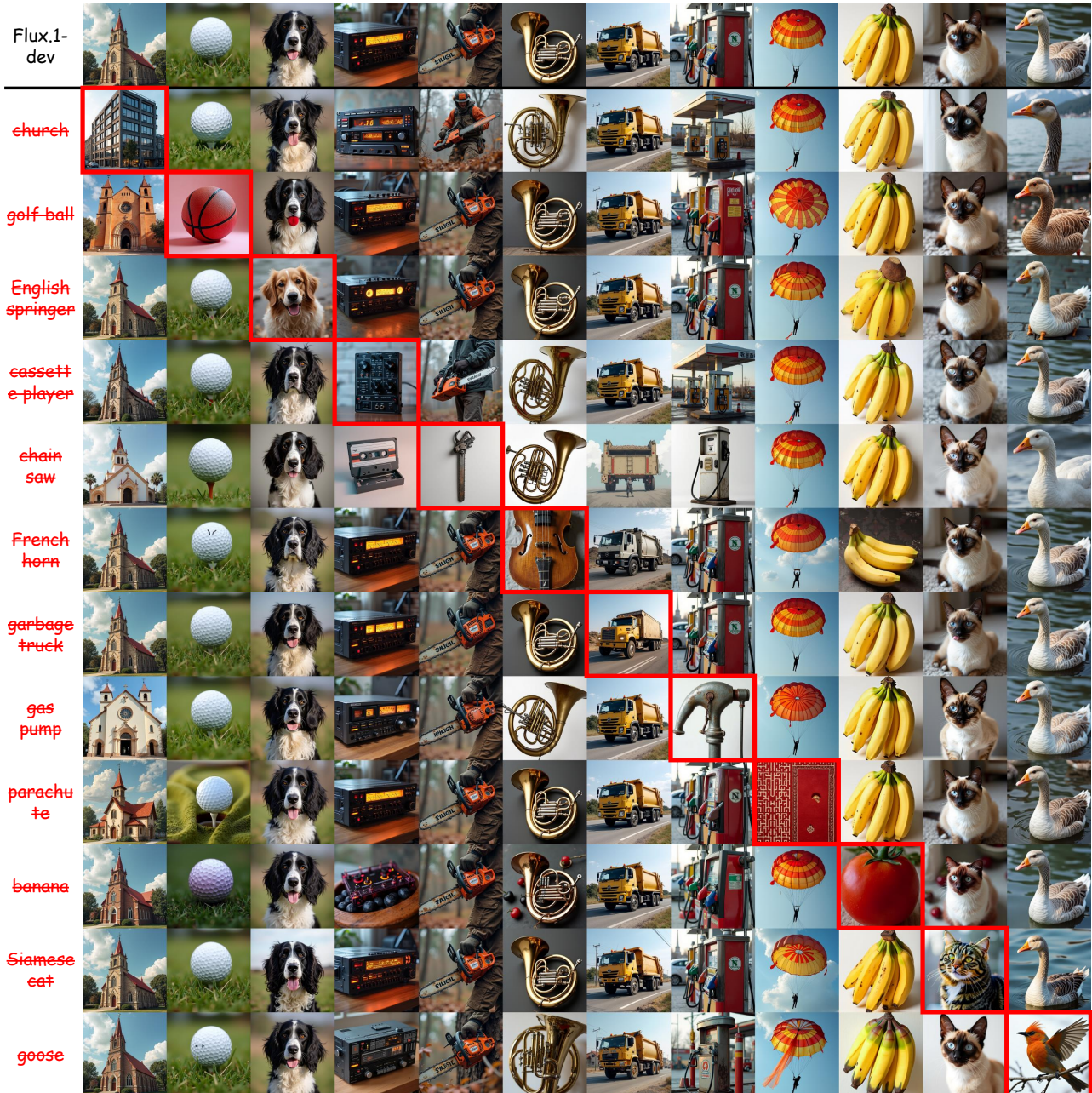


Figure 7. Additional visualization results for object erasure across erasure concepts and prompts used for generation. The image enclosed in the red box is the image containing the concept to be erased.

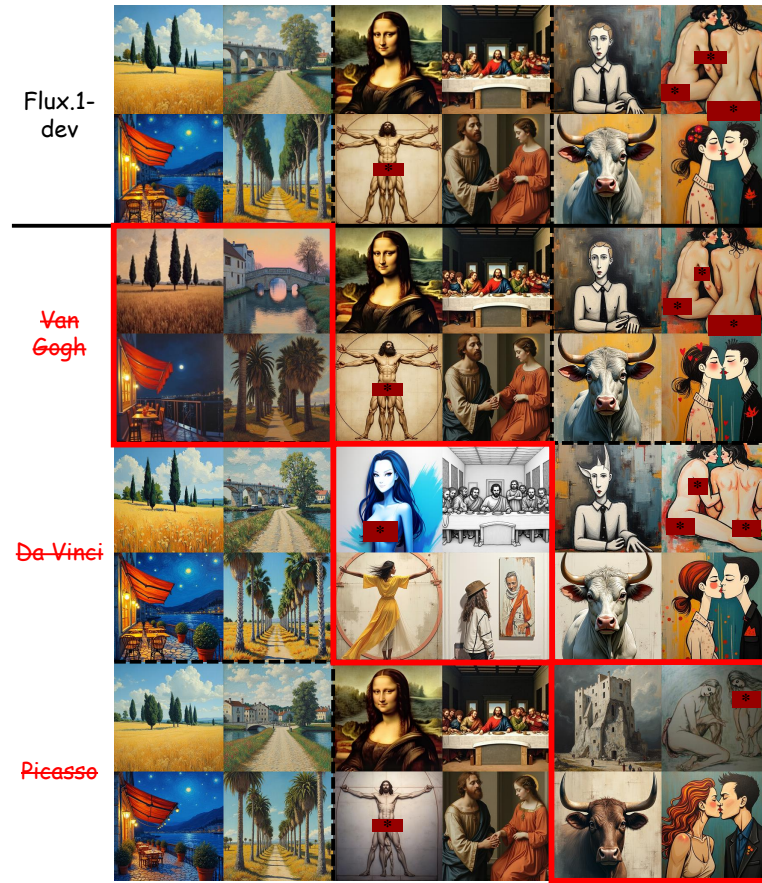


Figure 8. Additional visualization results for artist style erasure. The image enclosed in the red box is the image containing the concept to be erased.



Figure 9. Additional visualization results about the ablation study of impact of erasure strength and threshold.